Multicongenic fate mapping quantification of dynamics of thymus colonization

Natalia Ziętara,[1]* Marcin Łyszkiewicz,[1]* Jacek Puchałka,[2] Katrin Witzlau,[1] Annika Reinhardt,[1] Reinhold Förster,[1] Oliver Pabst,[1,3] Immo Prinz,[1] and Andreas Krueger[1]

[1]Institute of Immunology, Hannover Medical School, D-30625 Hannover, Germany
[2]Dr. von Haunersches Kinderspital, University Children's Hospital, Ludwig Maximilian University, D-80337 Munich, Germany
[3]Institute of Molecular Medicine, RWTH Aachen University, D-52074 Aachen, Germany

Postnatal T cell development depends on continuous colonization of the thymus by BM-derived T lineage progenitors. Both quantitative parameters and the mechanisms of thymus seeding remain poorly understood. Here, we determined the number of dedicated thymus-seeding progenitor niches (TSPNs) capable of supporting productive T cell development, turnover rates of niche occupancy, and feedback mechanisms. To this end, we established multicongenic fate mapping combined with mathematical modeling to quantitate individual events of thymus colonization. We applied this method to study thymus colonization in CCR7$^{-/-}$CCR9$^{-/-}$ (DKO) mice, whose TSPNs are largely unoccupied. We showed that ~160–200 TSPNs are present in the adult thymus and, on average, 10 of these TSPNs were open for recolonization at steady state. Preconditioning of wild-type mice revealed a similar number of TSPNs, indicating that preconditioning can generate space efficiently for transplanted T cell progenitors. To identify potential cellular feedback loops restricting thymus colonization, we performed serial transfer experiments. These experiments indicated that thymus seeding was directly restricted by the duration of niche occupancy rather than long-range effects, thus challenging current paradigms of thymus colonization.

CORRESPONDENCE
Andreas Krueger:
Krueger.Andreas@
mh-hannover.de
OR
Natalia Ziętara:
Natalia.Zietara@
med.uni-muenchen.de

Abbreviations used: CMJ, cortico-medullary junction; DKO, CCR7$^{-/-}$CCR9$^{-/-}$ double knockout mice; DN, double negative; DP, double positive; ETP, early T-lineage progenitor; i.t., intrathymic; lin, lineage; LSFM, light-sheet fluorescence microscopy; MPP, multipotent progenitor; SCZ, subcapsular zone; TEC, thymic epithelial cells; TSP, thymus-seeding progenitor; TSPN, thymus-seeding progenitor niche.

At steady state, T cell development depends on continuous colonization of the thymus by BM-derived T-lineage progenitors. The nature of thymus-seeding progenitors (TSPs) has remained largely elusive. Various candidate populations have been proposed, including multipotent progenitors (MPPs) and lymphoid-restricted progenitors, as well as largely T-lineage–committed cells (Martin et al., 2003; Krueger and von Boehmer, 2007; Bell and Bhandoola, 2008; Wada et al., 2008; Schlenner et al., 2010; Luc et al., 2012). However, none of these BM-derived or circulating progenitors has a clearly detectable, phenotypically equivalent counterpart in adult thymus (Bhandoola et al., 2007). Consequently, it has been suggested that exposure to Notch signals in the thymus results in rapid phenotypic changes of TSPs (Krueger et al., 2006; Schwarz et al., 2007). We and others have shown that multiple progenitor populations, which can be minimally defined by expression of CD27 and CD135, contribute to T cell development (Serwold et al., 2009; Saran et al., 2010). Phenotypic characterization of TSPs is hampered by the low numbers of cells entering the thymus, whereas, in turn, failure to phenotypically identify TSPs has precluded direct quantification of thymus colonization and its regulation. It has been proposed that the irradiated adult thymus is colonized by as few as 10–200 cells per day (Wallis et al., 1975; Kadish and Basch, 1976; Scollay et al., 1986). Parabiosis experiments have suggested a 2–3% daily turnover of cells within the progenitor niche at steady state (Donskoy and Goldschneider, 1992). Various assay systems have been applied to estimate the quantity of TSPs. Short-term transfers allow direct quantification

* N. Ziętara and M. Łyszkiewicz contributed equally to this paper.

The Rockefeller University Press $30.00
J. Exp. Med. 2015 Vol. 212 No. 10 1589–1601
www.jem.org/cgi/doi/10.1084/jem.20142143

The Journal of Experimental Medicine

of homing (Scimone et al., 2006; Gossens et al., 2009). However, analysis of early time points precludes distinction between true TSPs that enter the T-lineage developmental pathway and cells that home to the thymus, but fail to differentiate further once inside the thymus. In contrast, long-term transfers selectively permit detection of T-lineage progeny derived from TSPs, but, in this case, intrathymic proliferation and differentiation events preclude straightforward interpretation of data (Wallis et al., 1975; Kadish and Basch, 1976; Scollay et al., 1986). Recently, a combination of short-term transfer followed by analysis of T-lineage potential in vitro was applied to estimate TSP numbers (Zhang et al., 2014). However, in vitro differentiation assays are highly sensitive and might result in an overestimate of true TSPs (Schlenner and Rodewald, 2010; Richie Ehrlich et al., 2011).

Thymus colonization by BM-derived progenitors is tightly controlled. It depends on various adhesion molecules, including integrins and P-selectin ligand (Lepique et al., 2003; Rossi et al., 2005; Scimone et al., 2006). In addition, chemokine receptors, particularly CCR7 and CCR9, are required for recruitment of BM-derived progenitors to the thymus (Krueger et al., 2010; Zlotoff et al., 2010). Of note, dependency on CCR7 and CCR9 is transiently alleviated after conditioning by irradiation (Zlotoff et al., 2011). To date, the mechanisms limiting progenitor input remain ill characterized. It has been suggested that receptivity of the thymus for progenitors is a periodic event, allowing for colonization approximately every 3.5 wk, possibly dependent on oscillating expression of P-selectin and CCL25 (Donskoy et al., 2003; Gossens et al., 2009). Furthermore, reconstitution experiments in IL-7R– and RAG-deficient mice suggested that thymus colonization is limited by a cellular feedback loop, in which the size of the DN2 and/or DN3 compartment likely restricted progenitor entry. However, the mechanisms underlying this feedback remain unknown.

In this study, we set out to quantitate the overall number of intrathymic microenvironmental niches capable of sustaining productive T cell development and to determine turnover rates of niche occupancy and feedback mechanisms. Extrathymic progenitors from CCR7$^{-/-}$CCR9$^{-/-}$ (DKO) mice have a severe defect in colonizing a postnatal thymus, resulting in low numbers of early T-lineage progenitors (ETPs) in these mice (Krueger et al., 2010; Zlotoff et al., 2010). This phenotype suggested that DKO mice constituted an excellent model to study colonization of the adult thymus. Indeed, nonmanipulated DKO mice were readily susceptible to thymus seeding. Using these mice in combination with multicongenic fate mapping of BM-derived progenitors revealed that the adult thymus contains ∼160 TSP niches (TSPNs), 6% of which are accessible to recolonization at steady state. Furthermore, consecutive transplantation of congenically tagged progenitors into DKO mice showed that niche occupancy by ETPs is likely to directly control access to these microenvironmental niches. Thus, our study provided a quantitative model of colonization of the postnatal thymus and the underlying mechanisms.

RESULTS

Thymus of CCR7$^{-/-}$CCR9$^{-/-}$ double knockout mice (DKO) is highly receptive for TSPs

To test the hypothesis that thymi of DKO mice are highly receptive for colonization by WT progenitors, BM-derived lineage-negative (lin$^-$) progenitors (CD45.1) were transferred i.v. into nonmanipulated DKO and WT recipients (CD45.2). Thymus cellularity was substantially increased in DKO mice after transfer of WT cells, suggesting that recipient thymocytes were not replaced by donor-derived cells (Fig. 1 A). WT mice were largely refractory to thymus seeding by donor-derived cells, displaying a chimerism of ∼0.2% at 21 d after transfer (Fig. 1, B and C). In contrast, in DKO recipients, ∼50% percent of all thymocytes were of donor origin (Fig. 1, B and C). Developmental progression of donor cells within DKO recipients was normal and comparable to WT recipients 21 d after injection as assessed by CD4 and CD8 surface stainings (Fig. 1 B).

Some lin$^-$ progenitors might first colonize BM before thymus seeding and might therefore generate a reservoir for its continuous colonization. Indeed, we detected slightly elevated frequencies (in the range of 1%) of donor cells in DKO spleen and BM compared with WT controls (Fig. 1 D). However, DKO recipients were also much more receptive after transfer of sorted CLPs, which were previously shown to give rise to a single wave of T cell development and do not colonize BM for extended periods of time (Scimone et al., 2006; Krueger and von Boehmer, 2007; Fig. 1, E and F). Of note, overall reconstitution by sorted CLPs was lower in both WT and DKO recipients when compared with lin$^-$ BM cells (0.03 vs. 0.23% and 15 vs. 54%, respectively).

The numbers of ETPs and DN2 cells, but not other thymocyte populations, correlate with thymus receptivity

Whereas thymi of DKO mice are almost devoid of ETPs and DN2 cells, they only display a twofold reduction in DN3 cell numbers and mild alterations in numbers of more mature thymocytes (Krueger et al., 2010). This subset distribution suggested that increased thymic receptivity was a result of paucity in ETP/DN2 cells rather than more mature thymocytes. To test this hypothesis, we assessed thymus seeding of CCR7$^{-/-}$ and CCR9$^{-/-}$ single-deficient mice, which display intermediate phenotypes in subset cellularity. CCR7$^{-/-}$ mice were slightly more receptive to seeding by congenic (CD45.1 plus CD45.1/2) WT lin$^-$ progenitors displaying 3% donor-derived cells at 21 d after transfer when compared with 1% reconstitution of WT thymi (Fig. 2 A). Deficiency in CCR9 resulted in 11% donor-derived cells at 21 d after transfer, corresponding to an 11-fold increase in thymic receptivity when compared with WT recipients and a fourfold decrease when compared with DKO recipients (Fig. 2 A).

We correlated thymus receptivity to the abundance of various thymocyte subsets, including ETPs, DN2, DN3, and DP cells, in thymi of single mutant and DKO mice. We identified a strong inverse correlation of thymus receptivity with ETP

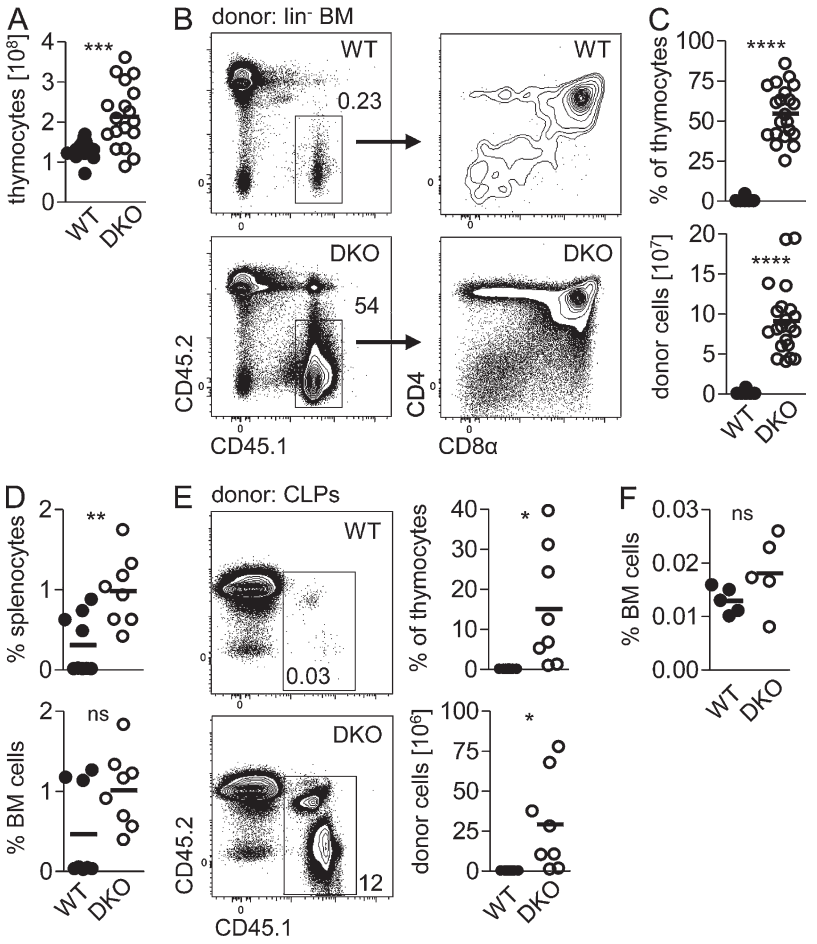

Figure 1. Thymi of CCR7$^{-/-}$CCR9$^{-/-}$ double deficient mice (DKO) are highly receptive for TSPs. Nonmanipulated WT and DKO recipient mice (CD45.2) were injected i.v. with congenic (CD45.1) WT lin$^-$ BM-derived precursors. (A) WT and DKO total thymocyte numbers 21 d after injection of WT lin$^-$ BM-derived precursors. (B) Analysis of WT and DKO recipient thymi 21 d after injection of WT lin$^-$ BM-derived precursors. Representative plots delineating donor and recipient cells (left) and CD8α versus CD4 profiles of WT donor-derived cells (right). (C) Percentages and absolute numbers of WT donor cells within all thymocytes of WT and DKO recipients. Pooled data from five independent experiments are depicted. (D) Analysis of WT donor cells in spleen (top) and BM (bottom) of WT and DKO recipient mice 21 d after transfer of lin$^-$ BM-derived progenitors. Pooled data from four independent experiments are depicted. (E) Analysis of WT and DKO thymi 21 d after injection of WT CLPs (CD45.1 and CD45.1/2). Representative plots of three independent experiments (left). Percentages and absolute numbers of donor cells within all thymocytes (right). (F) Analysis of WT donor cells in BM of WT and DKO recipient mice 21 d after transfer of CLPs. Data from three independent experiments. All recipient mice used in experiments shown in Fig. 1 were 4–6 wk old. Donor mice were 7–10 wk old. Each data point represents an individual mouse. Statistical analysis was performed using unpaired Student's *t* test, where ns, $P > 0.05$; *, $P \le 0.05$; **, $P \le 0.01$; ***, $P \le 0.001$; ****, $P \le 0.0001$.

and DN2 cell numbers (Fig. 2 B). In contrast, thymus receptivity did not correlate with numbers of DN3 and DP subsets.

Collectively, these data suggest that thymus receptivity depends on the presence of ETPs and DN2 cells, but not on other thymocyte subsets.

Spatial changes in thymic architecture do not accompany enhanced colonization of DKO thymus

TSPs enter the thymus from the bloodstream at the corticomedullary junction (CMJ; Petrie and Zúñiga-Pflücker, 2007). Therefore, alterations in thymus morphology might account for increased receptivity of DKO thymi. Immunohistological analysis of thymus sections from DKO and WT mice revealed an altered pattern of medullary regions in DKO mice. In sections, medullary areas (Ker5$^+$) were smaller in size, but their overall numbers were higher (Fig. 3, A and B). Combining reduced medullary area with increased numbers of medullary regions resulted in an increased ratio of cortical to medullary areas but an equal medullary perimeter per section (Fig. 3 B), suggesting that the overall size of the CMJ is not altered in DKO mice when compared with controls. To validate these conclusions, which were based on analysis in two dimensions, we used light-sheet fluorescence microscopy (LSFM) to assess thymus morphology in complete organs. Medullas were visualized by staining with UEA-1, followed by quantification of cumulative surface area of UEA-1$^+$ structures (Fig. 3 C and Video 1). DKO mice displayed a slightly increased total medullary area when compared with WT mice (Fig. 3 D, left). However, taking into account total thymus size, the relative size of medullary surfaces was comparable between WT and DKO thymi (Fig. 3 D, right). These data further support our conclusion that the size of the CMJ is not increased in thymi of DKO mice. Notably, the observed thymic architecture of DKO mice was highly reminiscent of that of CCR7$^{-/-}$ single-mutant mice (Misslitz et al., 2004; Ueno et al., 2004). Flow cytometric characterization of thymic stromal cells revealed reduced frequencies of medullary, but not cortical, thymic epithelial cells (TECs) or fibroblasts (Fig. 3 E). In addition, we found similar numbers of endothelial cells in DKO and WT thymi, suggesting that thymi of DKO mice do not contain an increased amount of vasculature (Fig. 3 E). Sorted nonhematopoietic cells did not display significant differences in mRNA expression of factors that mediate progenitor recruitment and survival, such as *Ccl19*, *Ccl21a*, *Ccl25*, *Selp* (P-selectin), and *Flt3l* (Fig. 3 F). Furthermore, we analyzed the distribution of cortical CD25^{hi} (DN2/DN3) thymocytes. In contrast to WT mice, which display an enrichment of DN2/DN3 cells at the subcapsular zone (SCZ), DKO mice

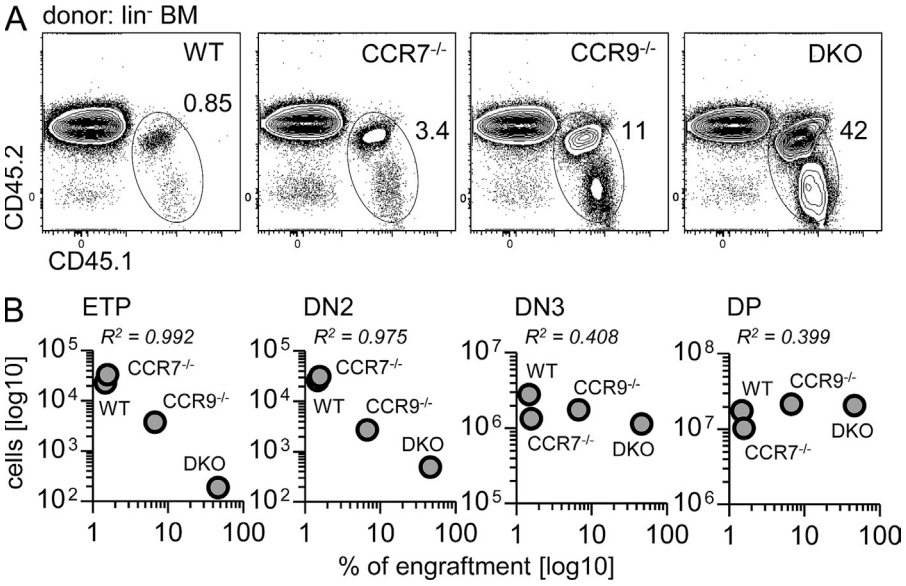

Figure 2. Thymus receptivity correlates with numbers of ETP and DN2 thymocytes. (A) Analysis of WT, CCR7$^{-/-}$, CCR9$^{-/-}$, and DKO thymi 21 d after transfer of congenic (CD45.1 and CD45.1/2) WT lin$^-$ BM precursors. Representative plots of two independent experiments, n = 6–8 for each genotype. (B) Correlation between abundance of recipient thymocyte populations and thymus receptivity, depicted as percentage of engraftment. Recipient mice were 4–11 wk old. Donor mice were 7–8 wk old. Each data point represents an average of six to eight mice/genotype from two independent experiments. R^2 = coefficient of correlation.

showed an equal distribution of these cells, similar to what has been described for CCR9$^{-/-}$ mice (Benz et al., 2004; Fig. 3, A and G). In summary, the thymic architecture of DKO mice combines the key features observed in CCR7$^{-/-}$ and CCR9$^{-/-}$ mice. Thus, we conclude that alterations in thymus morphology are unlikely to account for the massive increase in thymus receptivity of DKO mice when compared with either single mutant or WT mice.

Considering the profound increase in total thymus cellularity of DKO thymi 21 d after transfer of WT BM-derived progenitors, we determined whether the presence of large numbers of WT thymocytes was able to induce morphological changes toward a WT-like thymic architecture. To this end, we injected eGFP-tagged lin$^-$ BM-derived progenitors into WT and DKO recipient mice and analyzed thymic sections 21 d later. Donor-derived cells predominantly localized to the medullary regions and to medulla-proximal regions of the cortex, as expected after 21 d of developmental progression (Fig. 3 H). After this period of time, we did not observe any gross changes in thymic architecture of DKO recipients. Therefore, WT-like thymic morphology fails to be induced in adult DKO mice even when up to 50% of thymocytes are CCR7 and CCR9 sufficient.

T-lineage reconstitution in DKO mice is independent of progenitor exit from circulation

Thymus receptivity might be controlled at various nonmutually exclusive levels. It may be regulated via restriction of transit of progenitors from the circulation into the thymic microenvironment, via presence of a defined number of microenvironmental niches and/or via facilitating rapid proliferation of TSPs. To test whether transition from blood stream to the thymic microenvironment contributes to increased receptivity of DKO thymi, we assessed T cell development after direct administration of progenitors into the thymus. Intrathymic transfer of WT congenic lin$^-$CD117$^+$CD135$^+$ BM-derived progenitors into DKO mice resulted in chimerism of ∼40% when compared with 8% of WT mice (Fig. 4, A and B). Thus, in DKO mice, i.t. administration of progenitor cells resulted in equivalent levels of donor-derived T cell development when compared with i.v. administration, whereas in WT recipients i.t. administration resulted in higher levels of reconstitution when compared with the i.v. route. These data indicate that the receptive state in DKO mice is independent of active transition of progenitors from circulation to the thymic microenvironment and suggest that higher degrees of chimerism might be prevented by competition within more mature thymocyte populations. In contrast, in WT mice it is possible that i.t. transfer provides a competitive advantage over endogenous circulating TSPs.

To investigate whether faster proliferation rates of WT progenitors contributed to high donor chimerism within the DKO thymus, we tested incorporation of BrdU after a single 4-h pulse 14 and 21 d after transfer. At 14 d after transfer, donor-derived cells displayed slightly increased BrdU incorporation in DKO recipients when compared with controls, whereas no differences were observed after 21 d (Fig. 4 C). Minute frequencies of donor-derived cells, especially in WT recipients, precluded analysis of proliferation rates at earlier time points.

Thus, we conclude that intrathymic proliferation may in part contribute to enhanced T-lineage reconstitution in DKO mice, whereas active transition from circulation to the thymus appears to play a very limited role. These data suggest that availability of microenvironmental niches may to a large extent account for increased thymic receptivity of DKO mice.

Quantification of the adult thymus progenitor niche using multicongenic fate mapping

Next, we sought to determine the number of available microenvironmental TSPNs in DKO and WT mice. We hypothesized that this number corresponded directly to the number

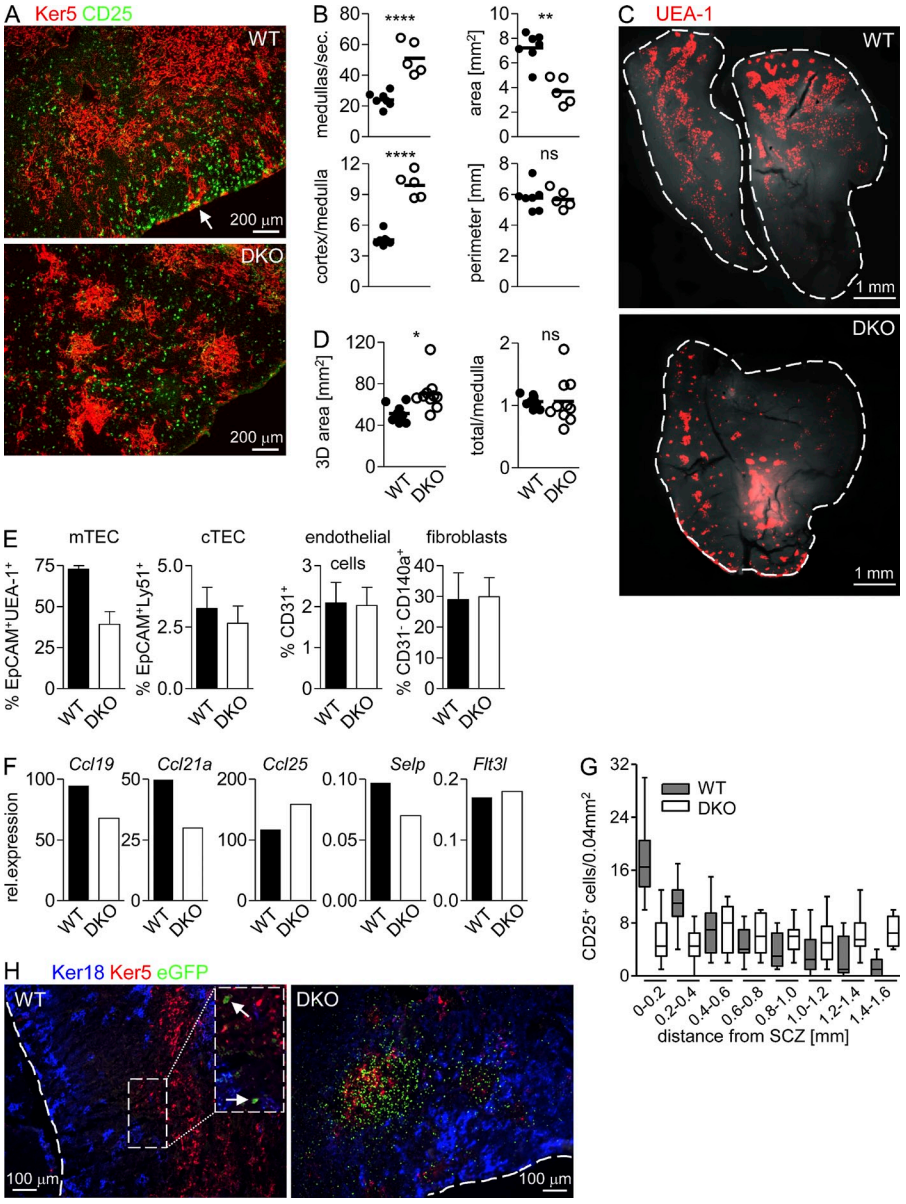

Figure 3. Thymic architecture of DKO recipient mice remains altered after WT progenitor entry. (A–G) Analysis of WT and DKO thymi without prior transfer. (A) Immunofluorescence microscopy of thymus cryosections from WT and DKO mice. Sections were stained with anti-cytokeratin 5 (Ker5, red) and anti-CD25 (green) antibodies. Arrowhead indicates accumulation of $CD25^{hi}$ cells (DN2 and DN3 thymocytes) at the SCZ of WT thymus. Representative sections of three to four thymi/genotype from two independent experiments are shown. (B) Quantification of medullas per section (sec.), their total area, perimeter and cortex to medulla ratios on cryosections of WT and DKO mice. Each dot represents one section of an entire thymus per mouse analyzed in two independent experiments. Statistical analysis was performed using unpaired Student's *t* test, where ns, $P > 0.05$; *, $P \leq 0.05$; **, $P \leq 0.01$; ****, $P \leq 0.0001$. (C) Light-sheet fluorescence microscopy (LSFM) of WT and DKO thymi. Medullas were labeled with UEA-1 (red). Representative images of virtual sections of five mice/genotype analyzed in two independent experiments are depicted. (D) Quantification of 3D areas of medullary regions (left) visualized by LSFM and their contribution within total thymic surface area (right). (E) Frequencies of mTECs ($CD45^-EpCAM^+UEA\text{-}1^+$), cTECs ($CD45^-EpCAM^+Ly51^+$), endothelial cells ($CD45^-CD31^+$), and fibroblasts ($CD45^-EpCAM^-CD31^-CD140a^+$) shown as percentage of nonhematopoietic cells ($CD45^-$). Pooled data from three independent experiments are depicted. $n = 3$–6/genotype. Data are represented as mean + SEM. (F) Gene expression analysis of sorted nonhematopoietic cells of WT and DKO mice by qRT-PCR. mTECs were analyzed for expression of *Ccl19* and *Ccl21a*, cTECs were analyzed for expression of *Ccl25*, thymic endothelial cells were analyzed for expression of P-selectin (*Selp*), and fibroblasts were analyzed for expression of *Flt3l*. Experiments were performed with RNA samples isolated from 5–7 pooled thymi for each genotype. Data from one representative experiment are depicted. (G) Quantification of distance of $CD25^+$ cells from SCZ. 200 × 1,600 µm areas were defined on two different regions of section (two random sections for two mice per genotype from two independent experiments as shown in A) using ImageJ software. $CD25^+$ cells were counted on 200 × 200 µm squares. Data are represented as mean ± SEM. (H) Immunofluorescence microscopy of thymus cryosections from WT and DKO recipient mice 21 d after transfer of eGFP-tagged BM precursors. Sections were stained with anti-cytokeratin 18 Ab (Ker18, blue) and anti-cytokeratin 5 (Ker5, red) to visualize thymic cortex and medulla. Arrowheads indicate single eGFP-positive cells (green). Representative sections from three mice for each genotype in one experiment are depicted. Mice used for experiments depicted in Fig. 3 were 4–6 wk old. Donor mice in H were 11 wk old.

of TSPs productively colonizing the thymus, i.e., giving rise to T-lineage progeny, at a given time point. To quantitate productive thymus seeding, we devised an approach of multicongenic fate mapping. To this end, we generated mouse strains expressing various combinations of congenic markers and/or reporter genes as tags allowing flow cytometric separation of cells of up to 12 distinct origins (Fig. S1 and Table S1; Buchholz et al., 2013). A Monte-Carlo simulation–based algorithm was generated to derive the number of TSPNs from the number of tags missing from donor-derived progeny (Fig. S2 A). This simulation was adopted from a method for estimating the number of bacteria founding an infection (Lim et al., 2014). It is based on the assumption that each TSP has the same capacity to populate a TSPN, irrespective of its congenic tag. Under this assumption, the probability that a TSP with a given tag populates a TSPN is proportional to the fraction of TSPs carrying this tag in the input population. In this scenario, low numbers of niches and/or the presence of tags with

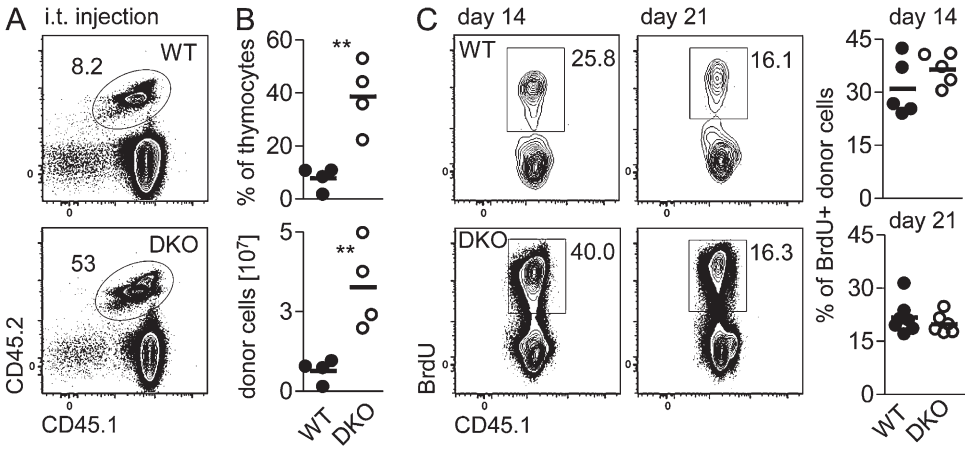

Figure 4. T-lineage reconstitution in DKO mice is independent of progenitor exit from circulation and intrathymic proliferation. (A) Analysis of thymi of WT and DKO recipient mice (CD45.2) 21 d after i.t. transfer of WT BM precursors (CD45.1/2). Representative plots of two independent experiments are depicted, $n = 4$. (B) Percentages and absolute numbers of donor cells within all thymocytes from experiments shown in A. (C) Analysis of BrdU incorporation in donor cells 14 and 21 d after i.v. injection of lin^- BM-derived precursors (CD45.1) into WT and DKO recipients (CD45.2). Density plots (left) and percentage of BrdU-positive cells within all donor cells (right). Recipient mice were 5 wk old. Donor mice were 8 wk old. Each data point represents one mouse. Data are representative of two independent experiments. Statistical analysis was performed using unpaired Student's *t* test, where **, $P \leq 0.01$.

low frequencies in the input population should result in failure of some tags to be recovered from donor-derived progeny. Consequently, the mixture of tags had to be composed depending on the suspected number of TSPNs. Counting missing tags then enabled assessment of the number of niches by simulating, several times, colonization events for a given number of TSPNs and then counting cases whenever the result of the simulation was equal to that of the experiment. Performing this procedure for a range of TSPN numbers and averaging the counts permitted identification of a range of most probable TSPN numbers provided that thymus seeding was restricted to a discrete colonization event. Pulse-chase experiments had shown that direct thymus colonization after transfer was essentially complete after 4 h (Spangrude and Weissman, 1988). Thus, circulating cells did not contribute detectably to a potentially extended phase of colonization. Furthermore, defined mixtures of BM-derived progenitors ($lin^-CD117^+CD135^+$), which lack the capacity of long-term engraftment of BM, were used in most fate mapping experiments, thus restricting the generation of a BM-resident source of TSPs. Finally, all donor-derived populations recovered displayed similar developmental progression as assessed by surface staining of CD4 and CD8, with most cells being at the DP and CD4 SP stages and very few DN cells detectable (Fig. S2 B). This finding suggested that all niches were occupied within a similar time frame and that loss of tags below the limit of detection indeed reflected failure to occupy a niche rather than a mere developmental delay. Differential analysis of tags at the DN and DP stages showed that DN and DP cells consistently contained a similar distribution of tags, with no tags being selectively present in DN cells but absent from DP cells. This analysis indicated that most, if not all, donor-derived cells originated from one discrete colonization event defined as within 4 h of transfer. In addition, experiments were designed in a way that the total number of transferred cells corresponded to saturating levels, which were originally determined to be in the range of 20×10^6 total BM cells (Foss et al., 2002). Accordingly, $4.5–15 \times 10^4$ $lin^-CD117^+CD135^+$ progenitors, which were previously reported to contain all TSPs and constitute ~0.5% of total BM were transferred (Serwold et al., 2009; Saran et al., 2010). T-lineage potential of CLPs in vivo was reported to be in the range of 1 in 20 and it is likely to be in a similar range for lymphoid-primed MPPs, suggesting that sufficient numbers of progenitors were present in the least frequent individually tagged populations (Kondo et al., 1997).

21 d after transfer of defined mixtures of congenically tagged progenitors into WT, DKO, and IL-7Rα–deficient recipients, the frequency of all donor-derived populations was determined (Table S1). IL-7Rα–deficient mice have been described to be particularly receptive for thymus seeding and were therefore chosen as positive control (Prockop and Petrie, 2004). The sensitivity of the experimental approach was assessed using a Delete-d Jackknife estimation of variance, which showed that the standard deviation of the predicted median did not exceed 20% (Fig. S2 C).

Donor-derived thymocytes in DKO recipients originated from ~160 TSPNs (Fig. 5 A). As these mice display high thymic receptivity in conjunction with barely detectable levels of ETPs and DN2 cells, as well as normal levels of key ligands for thymus homing, we suggest that this number is likely to be close to the maximum number of TSPNs available in an empty adult nonconditioned thymus. Interestingly, despite their high degree of responsiveness, IL-7Rα–deficient thymi contained only 24 TSPNs. 10 TSPNs were on average colonized by exogenous progenitors in WT mice, suggesting that at steady-state ~6% of TSPNs may be accessible. Furthermore, the distribution of individual progenitor tags in different WT recipients was more heterogeneous than in IL-7R$\alpha^{-/-}$

and DKO recipients (Fig. 5 B). This indicates that entry of BM-derived progenitors into the thymus is a stochastic event.

In conclusion, multicongenic fate mapping provided additional evidence that thymus receptivity directly depended on the availability of unoccupied intrathymic progenitor niches. Furthermore, our data suggested that the total number of microenvironmental progenitor niches in the adult thymus is as low as 160, 6% of which are replenished on average at steady state.

Conditioning of WT and IL-7Rα$^{-/-}$ mice through sublethal irradiation liberates TSPNs

Treatment with alkylating agents and/or irradiation is used as conditioning regimen before BM transplantation and affects thymus seeding and T-lineage reconstitution in multiple ways. Multicongenic fate mapping allowed us to directly assess the effect of irradiation on the availability of TSPNs. To this end, sublethally irradiated (4.5 Gy) WT, IL-7Rα$^{-/-}$ mice, and non-manipulated DKO mice received a defined mixture of BM-derived progenitors from multicongenic donors. 21 d after transfer, TSPN size was assessed using Monte Carlo simulation as described above. Thymi of sublethally irradiated WT mice contained a similar number of TSPNs as nonmanipulated DKO mice (Fig. 6, A and B). Furthermore, numbers of TSPNs in irradiated IL-7Rα$^{-/-}$ mice were increased by fourfold when compared with nonmanipulated IL-7Rα$^{-/-}$ mice (Fig. 6, A and B). These data indicate that conditioning through irradiation promotes thymus colonization by liberation of TSPNs and further support the hypothesis that the number of TSPNs identified in DKO mice likely corresponds to the near maximum of TSPNs in the adult thymus.

Occupancy of niches by ETPs regulates thymus seeding

Experiments with CCR7$^{-/-}$, CCR9$^{-/-}$, and DKO mice suggested that thymus receptivity was in part controlled by cellular feedback from ETPs and/or DN2 cells (Fig. 2). To investigate cellular feedback restricting progenitor entry at greater details, we again took advantage of the constitutive empty-niche status of DKO mice and multicongenic donor mouse strains. Such progenitors were transferred sequentially at 3-d intervals for 21 d, so that each recipient carried 8 distinct donor cell populations in total (Table S2). Thus, potential periodicity of thymus colonization could be directly assessed within an individual animal. 6 wk after the final transfer, spleens were analyzed for the presence of mature donor-derived T cells. At this time point, the vast majority of progeny of donor cells has dwelled in the periphery for at least 2 wk. Therefore, no bias based on post-thymic proliferation during maturation of recent thymic emigrants should be expected (Boursalian et al., 2004; Föhse et al., 2013). In consequence, frequencies of donor-derived T cells should directly reflect thymic entry of progenitors. Donor cells from transfers at day 0, 12, and 21 contributed the majority of donor-derived T cells with frequencies of ∼20% each (Fig. 7 A). In contrast, progenitors transferred at day 3, 6, 15, and 18 gave rise to ∼5% each and cells transferred at day 9 generated ∼10% of all donor-derived T cells. Thus, the frequency distribution of donor-derived splenic T cells from sequential transfers into DKO hosts reflected a periodicity of 9–12 d for thymus colonization of an initially empty recipient. Data from an analogous experiment using WT recipients showed a similar periodicity, although initial colonization was less efficient, presumably due to competition with endogenous TSPs (Fig. 7 B).

Given that the average life-time of ETPs was determined to be in the range of 10–12 d (Porritt et al., 2003), we conclude

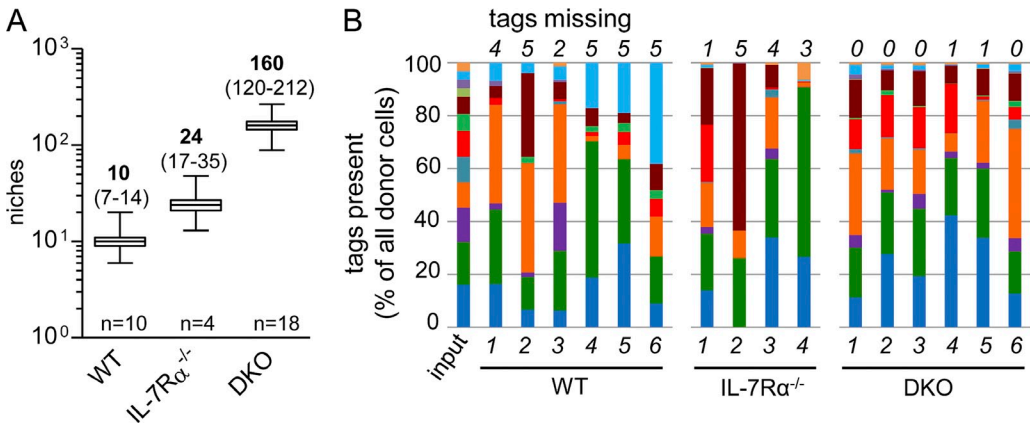

Figure 5. Quantification of early intrathymic niches using multicongenic fate mapping. Up to 12-code library of congenic/fluorescent tagged BM progenitors (multicongenic library) was generated by intercrossing of several mouse strains (Table S1). A mixture (4.8 × 10^4 to 15 × 10^4 cells/recipient mouse) consisting of defined ratios of such progenitors (Table S1, input [I], [II[, and [III]) was injected into nonmanipulated WT and DKO recipient mice (three independent experiments). Thymi of recipient mice were analyzed 21 d after progenitor injection. (A) Quantification of TSPNs was performed using an algorithm based on Monte Carlo simulation. Bold numbers above each boxplot represent the median number of TSPNs for each genotype. Numbers in brackets indicate 95% confidence intervals. Data from two experiments are depicted, n = 10 (WT), n = 4 (IL-7Rα$^{-/-}$), n = 18 (DKO). (B) Distribution of individual tags (each color represents one tag) within donor cells (100%) in different recipient mice 21 d after transfer. Input bar represents distribution of 12 tags within the progenitor mixture, which was injected into individual recipients at day 0. Numbers above each column indicate missing tags in each representative recipient; n = 6 (WT), n = 4 (IL-7Rα$^{-/-}$), n = 6 (DKO). Recipient mice were 4 to 7 wk old. Donor mice were 7 to 10 wk old.

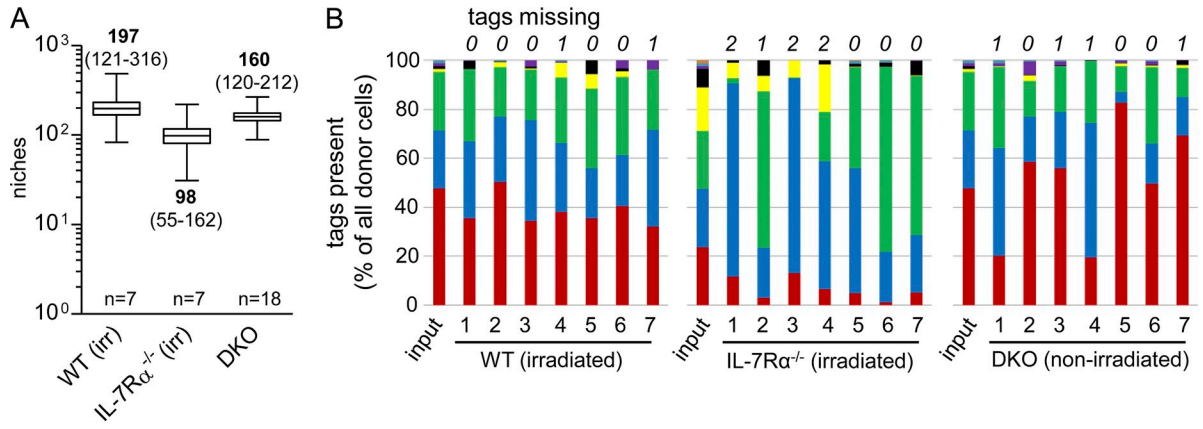

Figure 6. Conditioning of WT mice through irradiation fully liberates progenitor niches. Eight-code library of congenic/fluorescently tagged BM progenitors (multicongenic library) was generated by intercrossing of several mouse strains (Table S1). A mixture (4×10^6 lin$^-$ BM cells/recipient mouse) consisting of defined ratios of such progenitors (Table S1, input [IV]) was injected into sublethally irradiated (4.5 Gy) WT and nonmanipulated DKO recipient mice. A mixture (4.5×10^4 [V] and 13×10^4 [VI] of lin$^-$CD117$^+$Flt3$^+$ sorted BM cells/recipient mouse) consisting of defined ratios of such progenitors (Table S1, input [V] and [VI]) was injected into sublethally irradiated (4.5 Gy) IL-7R$\alpha^{-/-}$ mice. Thymi of recipient mice were analyzed 21 d after progenitor injection. (A) Quantification of TSPNs was performed as described for Fig. 5. Bold numbers above each boxplot represent the median number of TSPNs for each genotype. Numbers in brackets indicate 95% confidence intervals; $n = 7$ (WT irradiated, one experiment), $n = 7$ (IL-7R$\alpha^{-/-}$ irradiated, 2 experiments), $n = 18$ (DKO, 2 experiments). (B) Distribution of individual tags (each color represents one tag) within donor cells (100%) in different recipient mice 21 d after transfer. Input bar represents distribution of 8 tags within the progenitor mixture, which was injected into individual recipients at day 0. Numbers above each column indicate missing tags in each representative recipient; $n = 7$ (WT irradiated), $n = 7$ (IL7-R$\alpha^{-/-}$ irradiated), $n = 7$ (DKO). Recipient mice were 4–13 wk old. Donor mice were 7–10 wk old.

from these data that the occupancy of microenvironmental niches by ETPs is likely to constitute the predominant factor restricting access of progenitors to the adult thymus. These data also provide additional evidence that determination of TSPNs by multicongenic fate mapping, indeed, reflected a single colonization event rather than a continuous process.

DISCUSSION

Here, we have established CCR7$^{-/-}$CCR9$^{-/-}$ (DKO) mice as a model to study quantitative aspects of colonization of adult thymus without prior conditioning and cellular mechanisms restricting import of T lineage progenitors. Our data support a model, in which the average adult murine thymus contains ~160 microenvironmental niches for colonization by BM-derived progenitor cells. At steady state, ~6% of these niches can be replenished at any given time. Comparison of single-mutant and DKO mice indicated that thymus receptivity inversely correlated with numbers of ETPs and DN2 cells. Furthermore, microenvironmental progenitor niches can be refilled with a periodicity of 9–12 d. This number corresponds well to the lifetime of ETPs. Therefore, it is likely that niche occupancy is controlled by self-restriction and niches are liberated by developmental progression of ETPs occupying such niches.

Different strategies and mouse models have been used to study thymus colonization. Irradiation has been used to empty progenitor niches in order quantitate niches or "synchronize" colonization to analyze cellular feedback. However, irradiation causes multiple and difficult to control alterations in thymic architecture and cellular composition; it also alters expression of chemokines and cytokines, resulting in receptivity for progenitors that do not normally settle the adult thymus (Zubkova et al., 2005; Schwarz et al., 2007; Kenins et al., 2008). IL-7Rα–deficient mice also display a high degree of thymic receptivity (Prockop and Petrie, 2004). Although the overall composition of thymocytes by and large corresponds

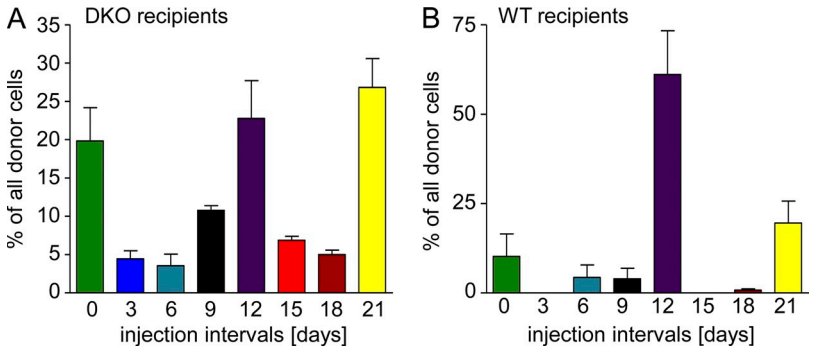

Figure 7. Occupancy of niches by ETPs regulates thymus seeding. Multicongenic BM-derived progenitors were injected into DKO recipient mice, one individual tag (10^6 of lin$^-$ BM cells/recipient mouse) every 3 d for 21 d. Analysis of donor-derived splenic T cells was performed 42 d after the final injection. (A) Quantification of donor cells within all splenocytes of DKO recipient mice. (B) Quantification of donor cells within all splenocytes of WT recipient mice. Data are representative of two independent experiments, $n = 7$–12 recipients/genotype. Recipient mice were 5 and 6 wk old. Donor mice were 7–8 wk old.

to that of WT mice in these mice, total thymic cellularity is massively reduced. However, small thymus size did not sufficiently explain our finding that nonmanipulated IL-7Rα$^{-/-}$ mice only contained 24 TSPNs, because preconditioning by irradiation was able to liberate additional TSPNs. In contrast to DKO mice, accessibility of TSPNs might not constitute the sole mechanism underlying increased thymic receptivity in IL-7Rα–deficient mice. Rather, it is conceivable that in these mice, WT TSPs compete favorably for IL-7 as survival cue. Thus, multiple factors are likely to contribute to the observation of high thymus receptivity, including accessibility of TSPNs, as well as intrathymic competitive advantages for prosurvival and proliferative cues.

Nonmanipulated mice represent the gold standard to assess quantity and regulation of progenitor niches. However, even taking into account periodicity of thymus colonization and use of recipients at an age of optimum receptivity did not result in progenitor entry compared with that of IL-7Rα$^{-/-}$ or DKO mice, thus precluding the use of WT mice in quantitative approaches (Gossens et al., 2009). DKO mice display normal thymic cellularity and a gross composition of thymocytes similar to WT mice (Krueger et al., 2010; Zlotoff et al., 2010). However, numbers of ETP and DN2 subsets are massively reduced and numbers of DN3 cells are somewhat reduced, due to a defect of canonical BM-derived progenitors to enter the thymus (Krueger et al., 2010; Zlotoff et al., 2010). Here, we showed that thymi of DKO mice share morphological features of both single mutant mouse strains with smaller but more numerous medullary regions and lack of accumulation of DN2/3 thymocytes at the SCZ. However, similar frequencies of endothelial cells, length and surface area of the CMJ as entry point for progenitors, and expression of homing molecules between DKO and WT mice suggest that altered thymic morphology does not significantly contribute to increased thymic receptivity in DKO mice. Therefore, we concluded that DKO mice represent a valid model for study colonization of the adult thymus.

We combined this model with an approach of combinatorial multicongenic fate mapping, which allowed us to discriminate up to 12 distinct populations of donor-derived cells. This approach circumvents pitfalls of conventional long- and short-term assays. Short-term homing assays have allowed recovery of comparatively large numbers of donor-derived cells (Mori et al., 2001; Scimone et al., 2006). Although there is no evidence that at steady state, in vivo only a fraction of cells entering the thymus finally ends up in the T-lineage; the majority of cells detectable in the thymus early after transfer is eventually lost (Mori et al., 2001). In contrast, analysis after extended periods of time ensures that only true T-lineage progenitors are taken into account. Moreover, the use of multiple tagged donor populations permitted direct quantification of the original input independent of intrathymic proliferation events. Of note, transfer of mixed populations of donor cells had already been reported four decades ago (Wallis et al., 1975; Ezine et al., 1984). However, limitation to two distinct donor populations permitted only rough estimates of the size of the TSP pool. Recently, short-term transfers have been combined with subsequent in vitro differentiation thus circumventing detection of false-positive cells that lack T lineage potential (Saran et al., 2010; Zhang et al., 2014). However, although this approach reliably excludes non–T-lineage progenitors, it does not discriminate between homed cells at large and those that indeed entered microenvironments required for productive T cell development.

Combinatorial fate mapping assays using DKO and WT recipients indicated the presence of a total of 160 thymic niches that can be colonized by BM-derived progenitors. 6% of these niches could be replenished, on average, in WT mice. Interestingly, the number obtained for DKO mice, corresponding to the total number of microenvironmental niches lies within the same range as in irradiated animals (Wallis et al., 1975; Kadish and Basch, 1976; Scollay et al., 1986; Spangrude and Scollay, 1990). These studies proposed a range from as few as 10 up to 170 progenitor cells as saturating number of TSPs to fully reconstitute an irradiated thymus. Combinatorial fate mapping analysis in irradiated recipients showed directly that conditioning through irradiation indeed liberated TSPNs, in addition to alterations in thymus size and cellular composition. These findings are in apparent contradiction with a recent study showing that irradiation restricted thymus colonization rather than promoting it as a consequence of loss of intrathymic availability of CCL25 (Zhang et al., 2014). Different doses of irradiation might account for the observed discrepancy, although the effect of lower irradiation doses on expression of intrathymic CCL25 remains to be explored.

Our data indicate that the availability of TSPNs directly depends on the presence of progenitors occupying these niches. These finding are in contrast to a model based on comparison between IL-7Rα–deficient and RAG-deficient mice, proposing that more mature, DN3, thymocytes provide direct feedback to restrict thymus colonization (Prockop and Petrie, 2004). However, the extent to which small thymus size and profound alterations in thymic morphology in RAG-deficient animals prevent thymus seeding has not been explored. Elevated levels of expression of *Psel* and *Ccl25* mRNA have been suggested to mediate increased thymus receptivity in IL-7Rα–deficient mice (Gossens et al., 2009). Interestingly, neither *Psel* nor *Ccl25* levels were elevated in DKO mice, suggesting that both molecular cues as well as niche occupancy itself may limit thymus colonization in a nonexclusive manner.

Comparison of the contribution of different donor populations showed that CLPs generated a lower degree of chimerism in both WT and DKO recipients when compared with lin$^-$ BM progenitors. This finding might imply that the thymus harbors progenitor-type specific TSPNs. However, it has been shown that CLPs only very transiently contribute to T cell development whereas MPPs, which are also present in lin$^-$ progenitors, sustain T cell development for extended periods of time even after i.t. administration (Saran et al., 2010; Schwarz et al., 2007). Thus, limited reconstitution of the DKO thymus by CLPs as assessed after 21 d is best explained by the transient nature of their progenitor activity.

Sequential transfer experiments in individual DKO mice revealed a periodicity of thymus colonization of 9–12 d. These data are consistent with a previous study showing that thymi of irradiated mice are receptive at 2-wk intervals after i.t. transfer (Foss et al., 2002). As all TSPNs in DKO mice can be considered empty, it is conceivable that this periodicity reflects duration of niche occupation at the individual niche level and is therefore likely to be masked at steady state. Notably, i.v. transfers and parabiosis experiments suggested longer refractory periods of 3–4 wk (Foss et al., 2001, 2002). Analysis of DKO mice at defined ages did not reveal any age-dependent alterations in thymus receptivity. These observations again point toward multiple independent mechanisms controlling thymus seeding and underscore the potential of DKO mice to dissect cellular and molecular mechanisms of colonization of the adult thymus.

Recently, it has been reported that in the absence of cellular competition, intrathymic T cell development becomes autonomous and ultimately results in the formation of T cell leukemia (Peaudecerf et al., 2012; Martins et al., 2012, 2014). These findings highlight the critical role of intercellular communication, directly or via competitive niche occupation. Our findings complement these data by showing that "old" progenitors are not simply pushed away by newcomers, but are rather capable of restricting continual influx from BM. Thus, intercellular communication between early thymocytes at various times after entry into the thymus appears to be pivotal to ensure balanced T cell development. Furthermore, the concept of cellular competition in the thymus predicts that progenitors from DKO mice are less competitive when compared with their WT counterpart. Therefore, it will be interesting to test whether transplantation of WT thymi into DKO mice, and thus competition not only for cytokines but also for location, will result in donor-thymus autonomous T cell development and leukemogenesis.

MATERIALS AND METHODS

Mice. C57BL/6J mice (CD45.2), B6.SJL-*Ptprc*^{a}*Pepc*^{b}/BoyJ mice (termed B6 CD45.1 throughout this manuscript) and IL-7Rα–deficient mice (B6.129S7-*Il7rtm1Imx*/J) were purchased from Charles River or The Jackson Laboratory or bred at the animal facility of Hannover Medical School. (C57BL/6J x B6 CD45.1) F1 mice (CD45.1/CD45.2 heterozygous) were bred at the animal facility of Hannover Medical School (Hannover, Germany). CCR7$^{-/-}$ (Förster et al., 1999), CCR9$^{-/-}$ (Wurbel et al., 2001), and CCR7$^{-/-}$CCR9$^{-/-}$ (DKO) mice were backcrossed to the C57BL/6 background for at least eight generations. B6.Cg-Thy1 (B6.Thy1.1), B6.Tg(*Actb-eGFP*) reporter mice (Okabe et al., 1997), and B6.Tg(*Actb-eCFP*) reporter mice (Hadjantonakis et al., 2002) were bred at the animal facility of Hannover Medical School. F1 mice of different fluorescent reporter/congenic intercrosses were bred at the animal facility of Hannover Medical School. Animals were maintained under specific pathogen–free conditions. Mouse care and experimental procedures were performed in accordance with German animal welfare legislation under the approval of the local authorities (Niedersächsisches Landesamt für Verbraucherschutz und Lebensmittelsicherheit, LAVES).

Isolation of lin^{-} BM precursors. Lin^{-} cells were isolated from total BM by labeling of single cell suspensions with a lineage-specific purified rat-anti-mouse-IgG antibody cocktail (anti-CD4, anti-CD8, anti-CD19, anti-CD11b, anti-Gr-1, Ter-119, and anti-NK1.1, all from eBioscience) followed by incubation with sheep-anti-rat-IgG magnetic beads (Dynal; Invitrogen) and magnetic bead depletion of mature lineages. Lin^{-} BM cells were used directly for injection in some of the experiments or for further cell sorting. Donor mice used for isolation of lin^{-} cells were always 7–10 wk old.

Flow cytometry and cell sorting. Monoclonal antibodies specific for CD4 (RM4-5, GK1.5), CD8 (53–6.7), CD25 (PC61), CD44 (IM7), Gr-1 (RB6-8C5), erythroid cell marker (Ter-119), CD19 (1D3), CD11b (M1/70), pan-NK (DX5), CD45.1 (A20), CD45.2 (104), B220 (RA3-6B2), CD117 (2B8, ACK2), Sca-1 (E13-161.7), CD135 (A2F10), CD127 (A7R34), BrdU (3D4), were used as biotin, Pacific Blue, fluorescein isothiocyanate (FITC), Alexa Fluor 488, phycoerythrin (PE), peridinin chlorophyll protein-Cy5.5 (PerCP-Cy5.5), PE-Cy7, allophycocyanin (APC), APC-Cy7, or APC-eFluor780 conjugates. Antibodies were purified from hybridoma supernatants using standard procedures or were purchased from eBioscience, BD, or BioLegend. Common lymphoid progenitor (CLP) cells were sorted from lineage-depleted BM as: lin^{-}Sca-1^{+}CD117$^{lo/+}$CD127^{+}CD135^{+}. Samples were acquired on an LSRII (BD) and sorted on a FACSAria II (BD). Data were analyzed with FlowJo software, v.9.4.9 (Tree Star). For analysis, dead cells and debris were excluded by gating of forward and side scatter. Sorted cells were of 98% or higher purity, as determined by reanalysis.

Intrathymic transfers. Mice (5 wk) were anesthetized with Ketamin/Rompun (Albrecht GmbH/Bayer; 10 mg/ml/0.04%/mouse in 150 µl) via i.p. injection and fixed in dorsal recumbency. A small, 4–5 mm transverse incision was made in the skin over the first intercostal space perpendicular to the sternum so that the second rib could be observed clearly. The needle entrance position was in the center of the first intercostal space and the needle angle at ∼90 degrees relative to the sternum. The injection volume was 20 µl. The proper injection depth was ∼3.5–4 mm according to age of the mouse and thymus size and thickness. The skin incision was closed using wound clips. Thymi were analyzed after 21 d for donor-derived cells.

BrdU incorporation. BrdU (Sigma-Aldrich) was injected i.p. (3 mg/mouse) 4 h before analysis. BrdU incorporation was analyzed using the FITC BrdU Flow kit (BD) according to the manufacturer's protocol. Samples were acquired on an LSRII (BD) and analyzed using FlowJo software (Tree Star).

Immunohistology. Thymi were excised from 5–6-wk-old age-matched mice, rinsed in PBS, embedded in Tissue-Tek O.C.T. (Sakura; Finetek), and frozen on dry ice. 8-µm cryosections were fixed for 10 min in ice-cold acetone and rehydrated in Tris-buffered saline with 0.05% Tween-20, blocked with 10% goat or mouse serum, and stained with the following antibodies at room temperature for 45 min. Rat anti-CD25 Alexa Fluor 488 (PC61 5.3; Invitrogen), polyclonal rabbit anti-cytokeratin 5 (Abcam), washed, and followed by staining with secondary goat anti–rabbit-Cy3 (Jackson ImmunoResearch Laboratories) for 45 min at room temperature. For analysis of thymi after injection of eGFP-tagged BM-derived precursors thymi were first fixed in 2% PFA and 30% sucrose overnight, washed in PBS, and embedded in O.C.T. medium. Sections were stained with monoclonal mouse anti–mouse cytokeratin 18 and biotin conjugated (Abcam), followed by incubation with streptavidin-Cy5 (eBioscience) and with rabbit anti-cytokeratin 5 as described above.

Immunohistological analysis of thymus sections was performed at room temperature using a motorized epifluorescence microscope (BX61; UPlanSApo; objective 10×/0.4) equipped with a fluorescence camera (F-View II) and CellSens software (Olympus). Quantification of CD25^{hi} cells was performed with ImageJ software (Schneider et al., 2012). Quantification of medullas and their perimeters and areas was performed using CellSens software (Polygon tool; Olympus).

Isolation and sorting of thymic nonhematopoietic cells. Thymi were excised from 5–6-wk-old age-matched mice, rinsed in PBS, cut into small pieces, collected in plain RPMI-1640, and incubated for 1 h at 4°C with gentle rotations to remove excess thymocytes. Supernatant was removed and

remaining tissue pieces were incubated with Collagenase D (0.2 mg/ml; Roche), Dispase Grade I (0.2 mg/ml; Roche), and DNase-I (0.025 mg/ml; Roche) 2 times for 15 min at 37°C with mixing every 5 min. Cells were collected on ice and incubated with 5 mM EDTA for 10 min. Nonhematopoietic cells were enriched after staining with rat anti–mouse CD45 antibody (30-F11; eBioscience), followed by incubation with sheep anti–rat magnetic beads (Invitrogen) and magnetic depletion. Cells were stained before FACS sorting using the following antibodies: anti-CD45 APC (30-F11; eBioscience), anti-EpCAM eFluor450 (G8.8; eBioscience), anti-Ly51 FITC (6C3; BD), anti-CD31 FITC (390; eBioscience), anti-CD140a PE (APA5; eBioscience), UEA-1 Rhodamine (Vector Laboratories). Cells were sorted on a FACSAria II with 130 µm nozzle at low speed as follows: cTECs, $CD45^-EpCAM^+Ly51^+$; mTECs, $CD45^-EpCAM^+UEA\text{-}1^+$; endothelial cells, $CD45^-CD31^+$; fibroblasts, $CD45^-EpCAM^-CD31^-CD140a^+$. Sorted cells were of 94–96% purity, as determined by reanalysis.

LSFM. Thymi were excised from 5-wk-old mice and fixed overnight at 4°C in PBS with 2% PFA and 30% sucrose. Further sample preparation was adapted from Renier et al. (2014) and Yokomizo et al. (2012). All steps were performed at room temperature. Samples were washed three times for 1 h in PBS, twice for 1 h in PBS with 0.2% Triton X-100 (Sigma-Aldrich), followed by two additional washing steps for 1 h in PBS with 1% Triton X-100. After overnight permeabilization in PBS with 1% Triton X-100, thymi were blocked in PBS with 0.5% Triton X-100, and 4% BSA for 3 d. After blocking, samples were washed twice for 1 h in PBS with 0.2% Tween-20 (Carl Roth) and stained for 4 d with UEA-1 Rhodamine (Vector Laboratories) in PBS with 0.2% Triton X-100 and 2% BSA. After staining, thymi were sequentially washed in PBS with 0.2% Tween-20 for 10, 30, 60, 120 min for 3 d, and finally in PBS for 15, 30, and 60 min. Sample clearing was performed as previously described (Ertürk et al., 2012) with minor modifications. Thymi were dehydrated in 50% tetrahydrofuran (THF; Sigma-Aldrich) for 2 h, 75% THF, and 100% THF for 3 h each, and finally overnight in 100% THF. Samples were cleared in dibenzylether (Sigma-Aldrich) and directly imaged after clearing was completed. Fluorescence images were acquired using a light-sheet microscope (Ultramicroscope II; LaVision BioTec) equipped with a sCMOS camera (Andor Neo) and a 2×/0.5 objective lens. 3D projections were analyzed with Imaris software (version 7.7.2; Bitplane).

qRT-PCR. RNA was prepared from samples with equal cell numbers using the RNeasy Mini kit according to the manufacturer's instructions (QIAGEN). Room temperature reaction was performed using SuperScript II Reverse transcription (Invitrogen) and $Oligo(dT)_{12\text{-}18}$ primers (Invitrogen) according to the manufacturer's protocol. Quantitative RT-PCR analysis of miRNA expression was performed using the following TaqMan probes (Applied Biosystems): *Ccl25*, Mm00436443_m1; *Ccl19*, Mm00839967_g1; *Ccl21a*, Mm03646971_gH; *Selp*, Mm01295931_m1; *Flt3l*, Mm00442801_m1. Fold differences were calculated using the ΔC_t method normalized to *Hprt* as housekeeping gene (Mm00446968_m1; Applied Biosystems). Reactions were performed using a StepOne Real-Time PCR System (Applied Biosystems).

Quantification of intrathymic niches using Monte Carlo simulation. DKO and WT nonmanipulated recipient mice (experiment I [WT 6 wk old, DKO 6 wk old], II [WT 4 wk old, DKO 4 wk old, IL-7Rα$^{-/-}$ 7 wk old], and III [WT 5 wk old, DKO 5 and 6 wk old]) were i.v. injected with defined mixtures (Table S1, input ratios/percentages) of BM progenitors, sorted as $lin^-CD117^{lo/+}CD135^+$ cells.

In the experiment number IV, V, and VI, empty intrathymic niches were generated by sublethal irradiation (4.5 Gy) of WT and IL-7Rα$^{-/-}$ recipient mice (DKO), and some WT recipients were nonmanipulated (experiment IV [WT 9 wk old, DKO 6 and 9 wk old], experiment V [IL-7Rα$^{-/-}$ 13 wk old], experiment VI [IL-7Rα$^{-/-}$ 4 wk old]). Cell numbers used in individual experiments are indicated in figure legends and Table S1. Proportions of different congenic populations are indicated in Table S1. Donors and recipients mice were sex-matched to prevent deletion caused by XY-chromosome incompatibility.

Thymi of recipient mice were analyzed 21 d after injection by flow cytometry. In total, 2.5×10^6 events were acquired per sample. Each individually tagged population was identified by its surface/fluorescent phenotype (Fig. S1) within total thymocytes of recipients and considered absent upon detection of <40 events (10 events were detected on average in these samples). On average, 4,800 events were detected in the least frequent populations considered present. Quantification of intrathymic niches was performed using an algorithm based on Monte Carlo smulation. This quantification was performed for each group (each experiment and each mouse genotype, nonmanipulated DKO, IL-7Rα$^{-/-}$ and WT, as well as irradiated WT in experiment IV, and irradiated IL-7Rα$^{-/-}$ in experiment V and VI), for which the experimental missing set was determined (i.e., the set containing, for each mouse in the group, the number of missing tags).

First, the number of accessible niches was set (niche-count). Subsequently, colonization was simulated by randomly determining which tag occupies every niche. The probability that a certain tag occupies a niche was proportional to its fraction in the tag pool. After the tag for every niche was determined, the number of tags that did not occupy any niche was determined and stored as the results of the simulation. This simulation was repeated, as many times as there were mice in the group, and the results of these were collected together to build one simulated missing set. If this set was equal to the set obtained experimentally for that group, the initially set number of niches was stored, as the result of one simulation of the invasion experiment. The simulation of the invasion experiment was repeated 10,000 times, so that between zero and 10,000 results were stored, constituting the result-set for given niche-count. This whole procedure was run iteratively starting from niche-count equal to 1 and increasing it by 1. The execution was stopped, when for five consecutive niche-counts, the result-set was empty and the niche count was greater than 130 (empirical value). The results-sets were merged together to build the final result-set for the group. If this set contained <10,000 elements, the number of repetitions of simulations of the invasion experiment was increased from 10,000 to a value that assured that the final result-set is of a length of at least 10,000. Finally, for each group 10,000 elements from the final result-set of each group were chosen randomly (with uniform probability), and these sub-sets were used to compute statistics for each group. The algorithm was implemented in R software suite (version 2.15.2; Team, 2012).

Repeated injections of multicongenic BM precursors. 5-wk-old DKO and WT nonmanipulated recipient mice were intravenously injected at 3-d intervals with equal amounts of an individually tagged population of lin^- congenic BM progenitors each (10^6 cells/injection day/recipient mouse) for 21 d (Table S2). Spleens of recipient mice were analyzed 6 wk after the final injection. Each individually tagged population was identified by its surface/fluorescent phenotype within total splenocytes of recipient mice.

Statistical analysis. All analysis except for the quantification of intrathymic niches was performed using GraphPad Prism software. Data are represented as mean + SEM or ± SEM, as indicated. Analysis of significance between 2 groups of mice was performed using unpaired Student's *t* tests, where ns, $P > 0.05$; *, $P \le 0.05$; **, $P \le 0.01$; ***, $P \le 0.001$; ****, $P \le 0.0001$.

To assess the efficiency of the simulation approach to estimate intrathymic niches, we performed Delete-d Jackknife estimation of variance. In this procedure a set of subsampled results is generated from the original result, by removing a predefined number of single measurements. This yields a set of $\binom{n}{k} = \frac{n!}{(n-k)!\times k!}$ results, where n is the group size and k the count of elements that were removed. Then the simulation is performed on each set member and the results are collected. As several results are obtained for each original result, the estimation of variance is possible. We performed this procedure for each group, while removing 25% of single experiments (rounded to the nearest integer) and running the simulation for every unique combination of missing clones (as single experiments lead often to the same number of missing clones, there are significantly fewer unique combinations than the total derived by the above formula). The result of such simulation was then weighted according to prevalence of the corresponding combination.

Online supplemental material. Figs. S1 and S2 contain data that support Figs. 1–7. Table S1 contains combinations of alleles used to generate multicongenic precursors library, their proportions and cell numbers used in individual experiments. Table S2 lists the sequence of injections used to determine cellular feedback which restricts thymus seeding. Video 1 contains LSFM analysis of WT and DKO thymi. Online supplemental material is available at http://www.jem.org/cgi/content/full/jem.20142143/DC1.

We thank Harald von Boehmer for critical reading of the manuscript and helpful discussions. We are grateful to Dr. Henrike Fleige and Stefanie Willenzon for help with immunohistology experiments, David Mzinza for help with LSFM, and Mathias Herberg for maintenance of mouse colonies. We would like to acknowledge the assistance of the Cell Sorting Core Facility of the Hannover Medical School supported in part by Braukmann-Wittenberg-Herz-Stiftung and German Research Foundation (DFG).

The work was supported by grants from the German Research Foundation (DFG; Emmy-Noether Program, KR2320/2-1; SFB738-A7; KR2320/3-1, and EXC62, "Rebirth"; to A. Krueger).

The authors declare no competing financial interests.

Author contributions: N. Ziętara, M. Łyszkiewicz, K. Witzlau, and A. Reinhardt performed experiments; N. Ziętara, M. Łyszkiewicz, J. Puchałka, A. Reinhardt, and A. Krueger analyzed data; N. Ziętara, M. Łyszkiewicz, J. Puchałka, A. Reinhardt, I. Prinz, and A. Krueger designed experiments; R. Förster and O. Pabst provided vital tools; N. Ziętara, M. Łyszkiewicz, J. Puchałka, and A. Krueger wrote the manuscript; A. Krueger conceived of the study.

Submitted: 14 November 2014
Accepted: 10 August 2015

REFERENCES

Bell, J.J., and A. Bhandoola. 2008. The earliest thymic progenitors for T cells possess myeloid lineage potential. *Nature*. 452:764–767. http://dx.doi.org/10.1038/nature06840

Benz, C., K. Heinzel, and C.C. Bleul. 2004. Homing of immature thymocytes to the subcapsular microenvironment within the thymus is not an absolute requirement for T cell development. *Eur. J. Immunol*. 34:3652–3663. http://dx.doi.org/10.1002/eji.200425248

Bhandoola, A., H. von Boehmer, H.T. Petrie, and J.C. Zúñiga-Pflücker. 2007. Commitment and developmental potential of extrathymic and intrathymic T cell precursors: plenty to choose from. *Immunity*. 26:678–689. http://dx.doi.org/10.1016/j.immuni.2007.05.009

Boursalian, T.E., J. Golob, D.M. Soper, C.J. Cooper, and P.J. Fink. 2004. Continued maturation of thymic emigrants in the periphery. *Nat. Immunol.* 5:418–425. http://dx.doi.org/10.1038/ni1049

Buchholz, V.R., M. Flossdorf, I. Hensel, L. Kretschmer, B. Weissbrich, P. Gräf, A. Verschoor, M. Schiemann, T. Höfer, and D.H. Busch. 2013. Disparate individual fates compose robust CD8+ T cell immunity. *Science*. 340:630–635. http://dx.doi.org/10.1126/science.1235454

Donskoy, E., and I. Goldschneider. 1992. Thymocytopoiesis is maintained by blood-borne precursors throughout postnatal life. A study in parabiotic mice. *J. Immunol*. 148:1604–1612.

Donskoy, E., D. Foss, and I. Goldschneider. 2003. Gated importation of prothymocytes by adult mouse thymus is coordinated with their periodic mobilization from bone marrow. *J. Immunol.* 171:3568–3575. http://dx.doi.org/10.4049/jimmunol.171.7.3568

Ertürk, A., K. Becker, N. Jährling, C.P. Mauch, C.D. Hojer, J.G. Egen, F. Hellal, F. Bradke, M. Sheng, and H.U. Dodt. 2012. Three-dimensional imaging of solvent-cleared organs using 3DISCO. *Nat. Protoc.* 7:1983–1995. http://dx.doi.org/10.1038/nprot.2012.119

Ezine, S., I.L. Weissman, and R.V. Rouse. 1984. Bone marrow cells give rise to distinct cell clones within the thymus. *Nature*. 309:629–631. http://dx.doi.org/10.1038/309629a0

Föhse, L., A. Reinhardt, L. Oberdörfer, S. Schmitz, R. Förster, B. Malissen, and I. Prinz. 2013. Differential postselection proliferation dynamics of αβ T cells, Foxp3+ regulatory T cells, and invariant NKT cells monitored by genetic pulse labeling. *J. Immunol.* 191:2384–2392. http://dx.doi.org/10.4049/jimmunol.1301359

Förster, R., A. Schubel, D. Breitfeld, E. Kremmer, I. Renner-Müller, E. Wolf, and M. Lipp. 1999. CCR7 coordinates the primary immune response by establishing functional microenvironments in secondary lymphoid organs. *Cell*. 99:23–33. http://dx.doi.org/10.1016/S0092-8674(00)80059-8

Foss, D.L., E. Donskoy, and I. Goldschneider. 2001. The importation of hematogenous precursors by the thymus is a gated phenomenon in normal adult mice. *J. Exp. Med*. 193:365–374. http://dx.doi.org/10.1084/jem.193.3.365

Foss, D.L., E. Donskoy, and I. Goldschneider. 2002. Functional demonstration of intrathymic binding sites and microvascular gates for prothymocytes in irradiated mice. *Int. Immunol*. 14:331–338. http://dx.doi.org/10.1093/intimm/14.3.331

Gossens, K., S. Naus, S.Y. Corbel, S. Lin, F.M. Rossi, J. Kast, and H.J. Ziltener. 2009. Thymic progenitor homing and lymphocyte homeostasis are linked via S1P-controlled expression of thymic P-selectin/CCL25. *J. Exp. Med*. 206:761–778. http://dx.doi.org/10.1084/jem.20082502

Hadjantonakis, A.K., S. Macmaster, and A. Nagy. 2002. Embryonic stem cells and mice expressing different GFP variants for multiple non-invasive reporter usage within a single animal. *BMC Biotechnol*. 2:11. http://dx.doi.org/10.1186/1472-6750-2-11

Kadish, J.L., and R.S. Basch. 1976. Hematopoietic thymocyte precursors. I. Assay and kinetics of the appearance of progeny. *J. Exp. Med*. 143:1082–1099. http://dx.doi.org/10.1084/jem.143.5.1082

Kenins, L., J.W. Gill, R.L. Boyd, G.A. Holländer, and A. Wodnar-Filipowicz. 2008. Intrathymic expression of Flt3 ligand enhances thymic recovery after irradiation. *J. Exp. Med*. 205:523–531. http://dx.doi.org/10.1084/jem.20072065

Kondo, M., I.L. Weissman, and K. Akashi. 1997. Identification of clonogenic common lymphoid progenitors in mouse bone marrow. *Cell*. 91:661–672. http://dx.doi.org/10.1016/S0092-8674(00)80453-5

Krueger, A., and H. von Boehmer. 2007. Identification of a T lineage-committed progenitor in adult blood. *Immunity*. 26:105–116. http://dx.doi.org/10.1016/j.immuni.2006.12.004

Krueger, A., A.I. Garbe, and H. von Boehmer. 2006. Phenotypic plasticity of T cell progenitors upon exposure to Notch ligands. *J. Exp. Med*. 203:1977–1984. http://dx.doi.org/10.1084/jem.20060731

Krueger, A., S. Willenzon, M. Lyszkiewicz, E. Kremmer, and R. Förster. 2010. CC chemokine receptor 7 and 9 double-deficient hematopoietic progenitors are severely impaired in seeding the adult thymus. *Blood*. 115:1906–1912. http://dx.doi.org/10.1182/blood-2009-07-235721

Lepique, A.P., S. Palencia, H. Irjala, and H.T. Petrie. 2003. Characterization of vascular adhesion molecules that may facilitate progenitor homing in the post-natal mouse thymus. *Clin. Dev. Immunol*. 10:27–33. http://dx.doi.org/10.1080/10446670310001598492

Lim, C.H., S. Voedisch, B. Wahl, S.F. Rouf, R. Geffers, M. Rhen, and O. Pabst. 2014. Independent bottlenecks characterize colonization of systemic compartments and gut lymphoid tissue by salmonella. *PLoS Pathog.* 10:e1004270. http://dx.doi.org/10.1371/journal.ppat.1004270

Luc, S., T.C. Luis, H. Boukarabila, I.C. Macaulay, N. Buza-Vidas, T. Bouriez-Jones, M. Lutteropp, P.S. Woll, S.J. Loughran, A.J. Mead, et al. 2012. The earliest thymic T cell progenitors sustain B cell and myeloid lineage potential. *Nat. Immunol.* 13:412–419. http://dx.doi.org/10.1038/ni.2255

Martin, C.H., I. Aifantis, M.L. Scimone, U.H. von Andrian, B. Reizis, H. von Boehmer, and F. Gounari. 2003. Efficient thymic immigration of B220+ lymphoid-restricted bone marrow cells with T precursor potential. *Nat. Immunol.* 4:866–873. http://dx.doi.org/10.1038/ni965

Martins, V.C., E. Ruggiero, S.M. Schlenner, V. Madan, M. Schmidt, P.J. Fink, C. von Kalle, and H.R. Rodewald. 2012. Thymus-autonomous T cell development in the absence of progenitor import. *J. Exp. Med*. 209:1409–1417. http://dx.doi.org/10.1084/jem.20120846

Martins, V.C., K. Busch, D. Juraeva, C. Blum, C. Ludwig, V. Rasche, F. Lasitschka, S.E. Mastitsky, B. Brors, T. Hielscher, et al. 2014. Cell competition is a tumour suppressor mechanism in the thymus. *Nature*. 509:465–470. http://dx.doi.org/10.1038/nature13317

Misslitz, A., O. Pabst, G. Hintzen, L. Ohl, E. Kremmer, H.T. Petrie, and R. Förster. 2004. Thymic T cell development and progenitor localization depend on CCR7. *J. Exp. Med*. 200:481–491. http://dx.doi.org/10.1084/jem.20040383

Mori, S., K. Shortman, and L. Wu. 2001. Characterization of thymus-seeding precursor cells from mouse bone marrow. *Blood*. 98:696–704. http://dx.doi.org/10.1182/blood.V98.3.696

Okabe, M., M. Ikawa, K. Kominami, T. Nakanishi, and Y. Nishimune. 1997. 'Green mice' as a source of ubiquitous green cells. *FEBS Lett*. 407:313–319. http://dx.doi.org/10.1016/S0014-5793(97)00313-X

Peaudecerf, L., S. Lemos, A. Galgano, G. Krenn, F. Vasseur, J.P. Di Santo, S. Ezine, and B. Rocha. 2012. Thymocytes may persist and differentiate without any input from bone marrow progenitors. *J. Exp. Med*. 209:1401–1408. http://dx.doi.org/10.1084/jem.20120845

Petrie, H.T., and J.C. Zúñiga-Pflücker. 2007. Zoned out: functional mapping of stromal signaling microenvironments in the thymus. *Annu. Rev. Immunol*. 25:649–679. http://dx.doi.org/10.1146/annurev.immunol.23.021704.115715

Porritt, H.E., K. Gordon, and H.T. Petrie. 2003. Kinetics of steady-state differentiation and mapping of intrathymic-signaling environments by stem cell transplantation in nonirradiated mice. *J. Exp. Med*. 198:957–962. http://dx.doi.org/10.1084/jem.20030837

Prockop, S.E., and H.T. Petrie. 2004. Regulation of thymus size by competition for stromal niches among early T cell progenitors. *J. Immunol*. 173:1604–1611. http://dx.doi.org/10.4049/jimmunol.173.3.1604

Renier, N., Z. Wu, D.J. Simon, J. Yang, P. Ariel, and M. Tessier-Lavigne. 2014. iDISCO: a simple, rapid method to immunolabel large tissue samples for volume imaging. *Cell*. 159:896–910. http://dx.doi.org/10.1016/j.cell.2014.10.010

Richie Ehrlich, L.I., T. Serwold, and I.L. Weissman. 2011. In vitro assays misrepresent in vivo lineage potentials of murine lymphoid progenitors. *Blood*. 117:2618–2624. http://dx.doi.org/10.1182/blood-2010-05-287102

Rossi, F.M., S.Y. Corbel, J.S. Merzaban, D.A. Carlow, K. Gossens, J. Duenas, L. So, L. Yi, and H.J. Ziltener. 2005. Recruitment of adult thymic progenitors is regulated by P-selectin and its ligand PSGL-1. *Nat. Immunol*. 6:626–634. http://dx.doi.org/10.1038/ni1203

Saran, N., M. Łyszkiewicz, J. Pommerencke, K. Witzlau, R. Vakilzadeh, M. Ballmaier, H. von Boehmer, and A. Krueger. 2010. Multiple extrathymic precursors contribute to T-cell development with different kinetics. *Blood*. 115:1137–1144. http://dx.doi.org/10.1182/blood-2009-07-230821

Schlenner, S.M., and H.R. Rodewald. 2010. Early T cell development and the pitfalls of potential. *Trends Immunol*. 31:303–310. http://dx.doi.org/10.1016/j.it.2010.06.002

Schlenner, S.M., V. Madan, K. Busch, A. Tietz, C. Läufle, C. Costa, C. Blum, H.J. Fehling, and H.R. Rodewald. 2010. Fate mapping reveals separate origins of T cells and myeloid lineages in the thymus. *Immunity*. 32:426–436. http://dx.doi.org/10.1016/j.immuni.2010.03.005

Schneider, C.A., W.S. Rasband, and K.W. Eliceiri. 2012. NIH Image to ImageJ: 25 years of image analysis. *Nat. Methods*. 9:671–675. http://dx.doi.org/10.1038/nmeth.2089

Schwarz, B.A., A. Sambandam, I. Maillard, B.C. Harman, P.E. Love, and A. Bhandoola. 2007. Selective thymus settling regulated by cytokine and chemokine receptors. *J. Immunol*. 178:2008–2017. http://dx.doi.org/10.4049/jimmunol.178.4.2008

Scimone, M.L., I. Aifantis, I. Apostolou, H. von Boehmer, and U.H. von Andrian. 2006. A multistep adhesion cascade for lymphoid progenitor cell homing to the thymus. *Proc. Natl. Acad. Sci. USA*. 103:7006–7011. http://dx.doi.org/10.1073/pnas.0602024103

Scollay, R., J. Smith, and V. Stauffer. 1986. Dynamics of early T cells: prothymocyte migration and proliferation in the adult mouse thymus. *Immunol. Rev*. 91:129–157. http://dx.doi.org/10.1111/j.1600-065X.1986.tb01487.x

Serwold, T., L.I. Ehrlich, and I.L. Weissman. 2009. Reductive isolation from bone marrow and blood implicates common lymphoid progenitors as the major source of thymopoiesis. *Blood*. 113:807–815. http://dx.doi.org/10.1182/blood-2008-08-173682

Spangrude, G.J., and R. Scollay. 1990. Differentiation of hematopoietic stem cells in irradiated mouse thymic lobes. Kinetics and phenotype of progeny. *J. Immunol*. 145:3661–3668.

Spangrude, G.J., and I.L. Weissman. 1988. Mature T cells generated from single thymic clones are phenotypically and functionally heterogeneous. *J. Immunol*. 141:1877–1890.

Team, R.C. 2012. R: A language and environment for statistical computing. R Foundation for Statistical Computing. Version 2.15.2.

Ueno, T., F. Saito, D.H. Gray, S. Kuse, K. Hieshima, H. Nakano, T. Kakiuchi, M. Lipp, R.L. Boyd, and Y. Takahama. 2004. CCR7 signals are essential for cortex-medulla migration of developing thymocytes. *J. Exp. Med*. 200:493–505. http://dx.doi.org/10.1084/jem.20040643

Wada, H., K. Masuda, R. Satoh, K. Kakugawa, T. Ikawa, Y. Katsura, and H. Kawamoto. 2008. Adult T-cell progenitors retain myeloid potential. *Nature*. 452:768–772. http://dx.doi.org/10.1038/nature06839

Wallis, V.J., E. Leuchars, S. Chwalinski, and A.J. Davies. 1975. On the sparse seeding of bone marrow and thymus in radiation chimaeras. *Transplantation*. 19:2–11. http://dx.doi.org/10.1097/00007890-197501000-00002

Wurbel, M.A., M. Malissen, D. Guy-Grand, E. Meffre, M.C. Nussenzweig, M. Richelme, A. Carrier, and B. Malissen. 2001. Mice lacking the CCR9 CC-chemokine receptor show a mild impairment of early T- and B-cell development and a reduction in T-cell receptor gammadelta(+) gut intraepithelial lymphocytes. *Blood*. 98:2626–2632. http://dx.doi.org/10.1182/blood.V98.9.2626

Yokomizo, T., T. Yamada-Inagawa, A.D. Yzaguirre, M.J. Chen, N.A. Speck, and E. Dzierzak. 2012. Whole-mount three-dimensional imaging of internally localized immunostained cells within mouse embryos. *Nat. Protoc*. 7:421–431. http://dx.doi.org/10.1038/nprot.2011.441

Zhang, S.L., X. Wang, S. Manna, D.A. Zlotoff, J.L. Bryson, B.R. Blazar, and A. Bhandoola. 2014. Chemokine treatment rescues profound T-lineage progenitor homing defect after bone marrow transplant conditioning in mice. *Blood*. 124:296–304. http://dx.doi.org/10.1182/blood-2014-01-552794

Zlotoff, D.A., A. Sambandam, T.D. Logan, J.J. Bell, B.A. Schwarz, and A. Bhandoola. 2010. CCR7 and CCR9 together recruit hematopoietic progenitors to the adult thymus. *Blood*. 115:1897–1905. http://dx.doi.org/10.1182/blood-2009-08-237784

Zlotoff, D.A., S.L. Zhang, M.E. De Obaldia, P.R. Hess, S.P. Todd, T.D. Logan, and A. Bhandoola. 2011. Delivery of progenitors to the thymus limits T-lineage reconstitution after bone marrow transplantation. *Blood*. 118:1962–1970. http://dx.doi.org/10.1182/blood-2010-12-324954

Zubkova, I., H. Mostowski, and M. Zaitseva. 2005. Up-regulation of IL-7, stromal-derived factor-1 alpha, thymus-expressed chemokine, and secondary lymphoid tissue chemokine gene expression in the stromal cells in response to thymocyte depletion: implication for thymus reconstitution. *J. Immunol*. 175:2321–2330. http://dx.doi.org/10.4049/jimmunol.175.4.2321